Bistatic Radar for Military Space Domain Awareness at Geosynchronous Orbits

Andrew Kintz[1], Gregory Hogan[1], Alexander Kobsa[1], Simon Garrington[2], Alexander Serrano[1], Sarah Welch[1], Robert Morrison[1], Selenia Ghio[3], Cees Bassa[4], Paul Harrison[2], Nick Wrigley[2], Nick Pallecaros[5], Isaac Lowe[6], Andy Torres[6], Delphine Cerutti-Maori[7], Joseph Usoff[1], Marco Martorella[8], Matern Otten[9], Faruk Uysal[9]

[1]MIT Lincoln Laboratory, USA; [2]Univ. of Manchester, GBR; [3]CNIT-RaSS, ITA; [4]ASTRON Netherlands Institute for Radio Astronomy, NLD; [5]Dstl, GBR; [6]US Space Command, USA; [7]Fraunhofer FHR, GER; [8]Univeristy of Birmingham, GBR and CNIT-RaSS, ITA; [9]TNO, NLD

andrew.kintz@ll.mit.edu, hogan@ll.mit.edu, alexander.kobsa@ll.mit.edu, simon.garrington@manchester.ac.uk, alexander.serrano@ll.mit.edu, swelch@ll.mit.edu, rmorrison@ll.mit.edu, selenia.ghio@cnit.it, bassa@astron.nl, paul.harrison@manchester.ac.uk, nick.wrigley@manchester.ac.uk, ngpallecaros@mail.dstl.gov.uk, isaac.lowe@usspacecom.mil, andres.torres.1@usspacecom.mil, delphine.cerutti-maori@fhr.fraunhofer.de, usoff@ll.mit.edu, m.martorella@bham.ac.uk, matern.otten@tno.nl, faruk.uysal@tno.nl

ABSTRACT

Long baseline bistatic radars herald enhanced sensitivity and metric accuracy for clustered objects in Geosynchronous (GEO) orbits and beyond. Radio telescope arrays in particular feature large apertures, low noise temperatures, and stable, synchronized clocks. Pairing radio-telescope arrays with high-power radars creates new opportunities for rapidly determining orbits, correlating closely spaced objects, and characterizing tumbling or maneuvering targets. In this paper we report on long baseline bistatic measurements using the Millstone Hill Radar (MHR) in the USA and receivers in multiple antennas of the e-MERLIN array in the United Kingdom and the Westerbork Synthesis Radio Telescope in the Netherlands. Providing basic information about the transmitted waveform enables multiple receivers to detect, identify and track multiple targets. Applying long coherent integration and combining polarizations further increases the target SNR and reduces the minimum detectable RCS. Specialized Doppler processing on tumbling targets enabled determination of rotation period and minimum target dimensions. The work here presented has been carried out as part of the Program of Work of the NATO SET-293 Research Task Group (RTG).

1.0 INTRODUCTION

1.1 Motivation and Space Domain Awareness (SDA)

NATO acknowledges that the space domain is increasingly important to the Alliance and Allies' security and prosperity. They recognize that space is becoming more crowded and contested and that satellites are vulnerable to emerging counterspace capabilities and intentions. Between 2019 and 2021 the combined operational space fleets of China and Russia have grown by 70 percent. This recent and continuing expansion follows a period of growth where China and Russia had increased their combined fleets by more than 200 percent [1]. Along with the growth of their space fleets, they have developed and tested a wide range of counterspace technologies. In response, NATO, in 2019, adopted a new Space Policy (updated in January 2022 [2]) and declared space an operational domain. One of four mission areas of the newly formed US Space Command is to defend U.S., Allied, and Partner Interests. Specifically, USSPACECOM, in coordination with Allies, the joint force, and inter-agency partners, will conduct combined space operations to protect our combined interests and secure critical capabilities. [3]. Space Domain Awareness (SDA)

encompasses the effective identification, characterization and understanding of satellites that could affect space operations, and is a top priority for the USSPACECOM. A key aspect of SDA is the ability to discover and characterize new threats as well as maintain custody of all known space objects, of any provenance.

Space Domain Awareness (SDA) is foundational to NATO and USSPACECOM's dynamic understanding of space activities in or near Geosynchronous orbits (GEO). A tactical awareness of satellite activity in this regime, to include maneuvering satellites and multiple satellites in close proximity, CSOs (closely spaced objects) is of great interest and concern. Ground-based optics and radars are the dominant sensors employed for this awareness, however, optical sensing is hampered by inclement weather and by solar exclusion periods where radar has a 24/7 capability. There are two main challenges to achieving SDA at Geosynchronous Earth Orbit (GEO) with radar: sensitivity and imprecise knowledge of target orbits.

Sensitivity: Loss of radar sensitivity is due to the extreme tracking distance, which is 36,000 km to the GEO belt. To increase the sensitivity of a monostatic radar, one must increase the transmit power, build a larger aperture, or reduce the system temperature of the sensor. The sensitivity is most affected by the aperture size, as sensitivity scales with the fourth power of the aperture diameter, but it is cost prohibitive to build large aperture radars, and engineering challenges impose an upper limit on the size and slew rate of such sensors [4]. However, an option to increase radar sensitivity is to consider a multistatic radar that uses current monostatic transmitters with existing large aperture radio telescopes as receivers.. There are numerous large diameter (>25 m) radio telescopes that can be paired with radars. Using radio telescopes as receiving elements is advantageous in several ways: in addition to their large size, 1) radio telescopes typically have low system temperatures, often an order of magnitude lower than a radar's, which further increases their sensitivity; 2) their pointing and tracking capabilities are well matched to GEO targets; 3) they are typically equipped with wide-band receivers allowing flexibility to pair with multiple transmitting radars; 4) they usually have excellent frequency standards (H-masers) allowing coherent bistatic observations; 5) there is potential for combining astronomical and radar observations calibration; and 6) radio telescopes regularly operate in accurately time-synchronized interferometric networks [5], [6].

Advanced Signal Processing: Radar operations at GEO require coherent integration of many radar pulses (100s to 1000s) to achieve adequate Signal-to-Noise (SNR) for detection and tracking of RSOs. Effective integration of these pulses requires they be aligned coherently or "in-phase" with the satellite trajectory which, in turn, requires a detailed understanding of the particular satellite orbit, that is typically described by an element set (ELSET) and can be supplied by various sources, for example Spacetrack.org. Effective detection, through coherent pulse integration, is a function of the accuracy of the element set which in turn is usually a measure of the element set age or staleness. Poor element set quality can result in poor or no satellite detection. This is particularly the case for small targets that require long integrations due to reduced signature.

A technique to overcome this inadequate knowledge of the satellite orbit is to hypothesize a number of"nearby" orbits to the element set and process (integrate) the radar returns using these hypothesized orbits and examine, or search across the different hypothesized orbits and determine which yields a detection. Further processing of the radar data using this new orbit enables accurate satellite tracking. An additional feature of this Multi-Hypothesis Search (MHS) technique is that multiple satellites, within the radar beam, can be detected since many different orbits are examined. These multiple satellites can then be tracked independently yielding multiple target trajectories which informs military SDA, in particular understanding behavior of maneuvering satellites in proximity to others.

Another advantage of increased bistatic sensitivity is the ability to use shorter integration intervals to examine the motion of a satellite, in particular ones that are rotating (maneuvering) or tumbling; which would indicate instability or malfunction. By integrating over short time intervals and examining the satellite Doppler response over longer time periods, one can deduce the rotation period and a minimum size for the object. This characterization of GEO targets is also a key component of military SDA.

1.2 Data Collections

In early 2020, NATO Science & Technology Organization (STO) initiated a multi-year Sensors, Electronics and Technology (SET) Research Task Group (RTG) (SET-293) to examine the use of bistatic and multistatic radar configurations for improved SSA of GEO by combining existing NATO partner assets in the USA and Europe. SET-293 has performed experiments to explore real-world limitations to the theoretical link-budget of such bistatic systems and to explore multi-target tracking and characterization. A graphic depicting the radar transmitters (Tx) and receivers (Rx) geometry for the experiments is shown in Figure 1.

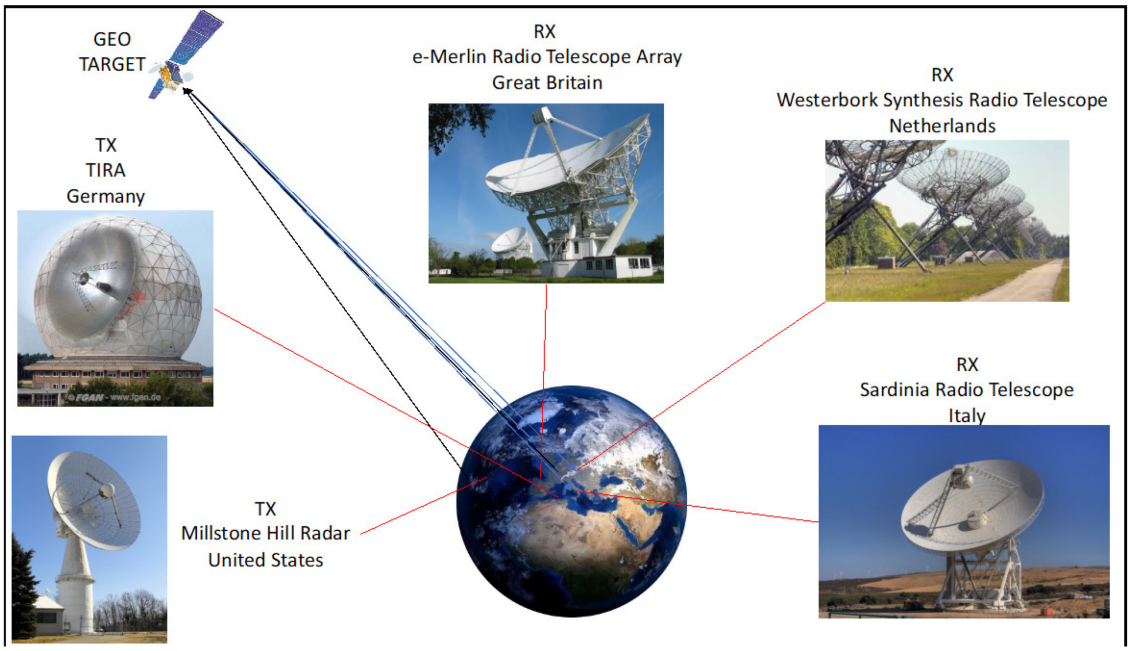

Figure 1: Radar multistatic experiment geometry depicting the radar transmitters illuminating a Geosynchronous satellite target and the radiotelescopes receiving the signal from the satellite.

One set of experiments paired the Millstone Hill Radar (MHR) in the USA with three receivers in Europe: the 64-meter Sardinia Radio Telescope (SRT) in Italy, a 25-meter antenna of the Westerbork Synthesis Radio Telescope (WSRT) in the Netherlands and multiple antennas of the e-MERLIN array, operated by The University of Manchester's Jodrell Bank Observatory (JBO) in the United Kingdom. e-MERLIN comprises 7 antennas with diameters from 25m to 76m and separations from 10km to 220km in the UK, used for high resolution radio astronomy imaging at centimeter wavelengths. The antennas are connected by a dedicated optical network to a central correlator and their coherence is maintained by a two-way RF timing signal on the same fiber. Additional bistatic experiments with smaller baselines were conducted in Europe between TIRA in Germany and the SRT and e-MERLIN radio telescopes. The sensors and their associated parameters are listed in Table 1.

The link budget is computed in terms of a Reference SNR for each receiver paired with MHR and TIRA. The reference monostatic SNR is 50 dB for MHR and 47 dB for TIRA, and it describes the maximum performance for a single pulse on a 0 dBsm target at 1000 km range. It is important to note that this link budget calculation assumes that the monostatic and bistatic RCS are equivalent. Additionally, the receiver gain, i.e. the difference between the monostatic sensitivity and the bistatic sensitivity is shown for each of the bistatic receivers in the last row of Table 1. The potential benefit of radio telescope receivers is apparent as even the modestly sized WSRT receiver is expected to show nearly 7 dB of receiver gain with MHR and 10 dB gain with TIRA due to its low system temperature as a receive-only system.

Initial experiments were conducted in 2020 and 2021 that verified data format understandings and then bistatic detections of GEO satellites. These results were presented at the European MicroWave Week conference in Milan, Italy in September of 2022 [7] and the NATO Specialists' Meeting on Space Situational Awareness in Interlochen, Switzerland October 2022. [8]

This paper will examine recent measurements that were conducted in the summer of 2022 through January of 2023. The goals of these collections were to examine 1) the response from additional JBO receivers, 2) coherent integration gain with longer collection times, 3) multi-target detection and tracking by viewing GEO'clusters' and 4) tumbling targets to explore Doppler processing to gain insights into target characterization.

2.0 PROCESSING OVERVIEW

2.1 Pulse Compression

The Millstone Hill Radar (MHR) is a 25.6-meter L-Band tracking radar located in Westford, Massachusetts in the United States. It is used primarily for deep space surveillance and is a contributing radar to the Space Surveillance Network (SSN) [9]. MHR is a coherent radar, meaning that the phase relationships between pulses are constant, allowing the integration of multiple pulses to increase the SNR. Many satellites are too small for single pulse detection and require coherent pulse integration to increase sensitivity, especially at GEO distances.

MHR operates at a center frequency of 1295 MHz and can transmit linear frequency modulated (LFM) pulses (chirps) up to 8 MHz in bandwidth with a peak power of 3000 kW. Unlike an unmodulated pulse, a chirp's bandwidth allows it to simultaneously have high range resolution and maintain a long enough duration for sufficient SNR [10]. The maximum pulse length is 1 millisecond, and up to 50 pulses can be transmitted per second, though the operating PRF is algorithmically determined based on the waveform and target range to prevent the received pulses from falling within the transmitter guard band.

Table 1: The sensor parameters and the link budgets are shown for MHR and TIRA monostatically and for each receiver paired with MHR and TIRA. The Reference SNR is the maximum performance on a 0 dBsm target at 1000 km range and is used to compute the RX Gain in the last row, i.e. the improvement in sensitivity of each bistatic receiver over MHR/TIRA monostatically. The WSRT parameters are for a single antenna in the array and two example e-MERLIN antennas are shown.

Parameter	MHR	TIRA	e-MERLIN (Lovell)	e-MERLIN (Knockin)	SRT	WSRT
	TX	TX	RX	RX	RX	RX
Lat/Lon (degrees)	42.6, 288.5	50.6 7.1	53.0, 357.4	52.8, 357.0	39.5, 9.2	52.9, 6.6
Antenna Diameter (m)	25.6	34	76	25	64	25
Center Frequency (MHz)	1295	1333	[1250-1750]	[1250-1750]	1295	1295
Ref. SNR (dB)	50	47	66	57	65	57
Rx Gain (dB)	–		16 / 19	7 / 10	15 / 18	7 / 10

In order to realize the range resolution and gain of a chirp waveform, the received pulse must undergo a technique known as pulse compression [11]. Once the pulses are compressed, the rest of the signal processing chain, such as coherent integration and target detection, can be executed. Pulse compression is accomplished by matched filtering the received samples with a stored replica of the transmitted pulse, and it is often implemented via a convolution operation. Since the radar cannot receive during the transmit window, it performs a range-gating step ahead of pulse compression by receiving during a small range window. The radar must therefore have an estimate of the target range in order to process the correct delays and detect the target.

Although TIRA did not participate for the collections described in this paper, it is included for completeness. The principle of the TIRA system is similar. The radar also operates in L-band at a slightly higher center frequency of 1333 MHz. TIRA uses binary phase shift keyed (BPSK) waveforms as transmit signal. The total pulse length, which is usually 1 millisecond long, is divided into N subpulses. The series of symbols employed to code the phase are arranged in a pseudo random noise sequence. The modulation number N, which ranges from 1 to 250, is set in real-time by the system depending on the SNR of the received signal. To compute the target range and Doppler frequency in real-time, TIRA uses a correlator quartet. The main beam of the ambiguity function is sampled at four distinct points around the expected range/Doppler position of the target (matched filter for different Doppler frequencies and ranges). From these values, the target parameters are estimated. The PRF of the TIRA system is approximately 30 Hz [12], [13], [14].

While a bistatic radar system could operate in the same manner, the bistatic experiments of SET-293 are fundamentally very different as the bistatic receivers are completely separate systems with no automated communication between the transmitter and receiver. The receiver must therefore record continuously throughout the duration of the experiment, as the receiver will not know when the transmitted pulses are arriving. The bistatic signal processing must occur offline in a post-processing pipeline.

The main assumption in these experiments is that the target ephemeris is known with reasonable accuracy such that the receiver can use the predicted position to control its pointing and record the transmitted pulses. The target motion is used during post-processing to first extract the receiver samples that contain the pulse, then generate the pulse replica for matched filtering and finally perform pulse compression. The pulse replica must account for the bistatic motion of the target exactly; for example, the transmitted pulse's chirp slope and time support will be transformed by the Doppler upon reflection from a moving target. All such factors are accounted for during pulse compression.

2.2 Coherent Processing – Multi-Hypothesis Search (MHS)

Even with the exquisite sensitivity provided by the bistatic sensors, coherent integration processing is often needed to generate a detection with sufficient SNR for a high precision track. To achieve the theoretical gain in SNR possible with coherent integration, namely a factor of N improvement, where N is the number of pulses integrated, the motion of the sensor's aimpoint must match that of the target with high accuracy. When there is mismatch due to imprecise ephemeris or other unaccounted for delays in the signal chain, the result is loss in integration gain. A factor specific to our bistatic experiment is the lack of real-time synchronization between sensors, which introduces additional time-varying delays. In particular, two of the dominant motion-error effects for orbiting space objects are range migration due to uncompensated radial velocity, and Doppler defocusing due to uncompensated acceleration. Radial velocity error can cause the signal from an object to migrate through multiple range resolution cells over the course of a coherent processing interval. As a result, the integrated signal energy does not accumulate to a single peak in range, but rather, is distributed across multiple range cells, leading to a reduction in the peak SNR and potentially precluding detection. Acceleration error is another factor that impairs detection when processing coherently. Acceleration mismatch is manifest in the signal data as a quadratic phase error across the pulses. Such phase error leads to well-known Doppler defocusing loss, where signal energy is spread across multiple Doppler resolution cells [15]. These losses, in combination, can lead to significant reduction in the SNR that prevents

detection of objects. Since the bistatic sensors in the experimental setup are not actively tracking, the effect of motion errors becomes more acute since the sensors must rely on ephemerides that lack the accuracy needed for coherent integration (the mismatch must be smaller than 1/20th of the wavelength, which is 1.15 cm for an L-band wavelength of 23 cm).

To overcome the effects of target-sensor motion mismatch, MIT Lincoln Laboratory has developed Multi-Hypothesis Search (MHS) signal processing. This processing applies multiple motion hypotheses to the data to determine the correction that maximizes target SNR. Key signal processing steps are the correction of linear range walk due to uncompensated radial velocity, and the correction of quadratic phase error due to acceleration. The MHS processing is capable of correcting motion errors for multiple objects within the sensor's field of view, which in general have different trajectories relative to each other and the sensor. MHS is applied after pulse compression to generate object detections. It includes logic for compacting signal detections at different hypotheses that are generated from the same object; this is necessary because neighboring acceleration hypotheses are highly correlated. The bounds for the motion search were selected based on typical uncertainties for space-object ephemerides, while the granularity of the search was chosen such that the correct hypothesis confines the object point response to within a single range-Doppler bin.

2.3 Experiment Description

Each bistatic experiment was scheduled with several days lead time between the MHR transmitter and the participating receiver(s). Large geostationary satellites (communications satellites) with visibility to all participating sensors were chosen for each of the experiments. Each sensor was responsible for obtaining the ephemeris of the chosen target, typically from open sources, and it was also responsible for propagating the ephemeris to the experiment time and pointing the sensor properly. For each collection, 2-3 satellites were chosen, and the data collection duration for each object was 5-10 minutes.

As there is no automated communication between sensors, planned recording times were determined ahead of time and controlled manually at each site. The transmitter center frequency and waveform bandwidth were also pre-determined so the receiver and recording system could be set to the appropriate bandwidth and sampling frequency. Furthermore, while many of the receivers are synchronized to highly accurate hydrogen maser clocks, GPS is the only time synchronization between the transmitter and receivers, and this was assumed to be sufficient for the purpose of these experiments.

NATO SET-293 members have conducted a number of experiments since early 2020 to establish procedures, data formats and test processing chains. The radio telescope receivers generally have multiple options for data acquisition to serve their own users. While it may be simpler to collect data in custom set-up such as an SDR receiver, many radio telescopes can record data in the VDIF format (*https://vlbi.org/vlbi-standards/vdif/)* used for VLBI around the world. The experiments with the e-MERLIN antennas have demonstrated the processing of VDIF data streams for radar applications. Table 2 lists the dates, the participating sensors, the NORAD ID number of the target satellites and the basic signal processing outcome of the successful experiments. Figure 2 show a picture of the satellites and longitudinal location. Other test experiments that did not result in target measurements are not included. For each of the target satellites, historical monostatic RCS measurements from MHR were used for comparison to the measured mono- and bistatic RCS during the experiment.

Table 2: Experiment dates, sensors, objects and the basic processing outcome of each experiment conducted.

Date	Sensors		Objects	Outcome
	Tx	Rx		
24/06/2022	MHR	JBO	41036	Target Detection
			33055	
			42950	
			43039	
14/12/2022	MHR	JBO, WSRT	36830	Target Detection, Long Integration Tumbling Object Characterization,
			41036	
			42950	
			43039	
			25126	
			40535	
			41590	
26/01/2023	MHR, TIRA	JBO, WSRT	25126	Target Detection, Long Integration
			43039	
			42950	
			36033	

3.0 EXPERIMENT RESULTS

3.1 Signal Processing for MHR Transmitting

Each bistatic data recording consisted of raw samples from an Analog to Digital (A/D) converter. The samples were converted to IQ and cross correlated with replica pulses. Cross correlation yields a sequence of pulses with equal time spacing of one pulse repetition interval (PRI) between them. Equal time spacing enables coherent integration with the Fast Fourier Transform (FFTs). FFTs were applied to the pulses across slow-time. The FFTs thus coherently integrated the pulses to form range-Doppler maps. Coherent integration provides sensitivity to perform various types of processing such as detection, tracking, or Doppler tomography and reconstruction.

Subsequent processing can take many paths. One option is to form many range-Doppler arrays with time-segments throughout the dataset. The range-Doppler arrays can be stacked into a 3D matrix known as a range-Doppler tensor [16]. The range-Doppler tensor can then be viewed from various faces. When viewing from one face of the Tensor, a maximum operation is taken along the collapsed dimension. The concept of looking through the Range-Doppler tensor is visualized in Figure 2. For example, if viewing the Tensor through the range-time face, the 2D output is the maximum amplitude for any Doppler at a given range and time. This data product is called range-superpulses, as it shows the targets' range versus time and benefits from coherent integration.

Looking through the Tensor's Doppler-time face yields the maximum amplitude for any range at a given Range-rate and time. This face shows the Doppler superpulses data product. Doppler superpulses show the targets' Doppler versus time. Stable targets yield simple traces in Doppler superpulse plots. These traces may separate stable targets at the same range but with different range-rates. Forming Doppler Superpulses is also an essential step for characterizing rotating or unstable targets. In making effective use of all available bandwidth in the radar data, Doppler superpulses render an all-inclusive spatial characterization of point-scatterers on the target over wide aspect diversity. By enhancing signal strength of point scatterers along sinusoidal trajectories, Doppler superpulse processing enables more accurate estimation of rotational motion parameters.

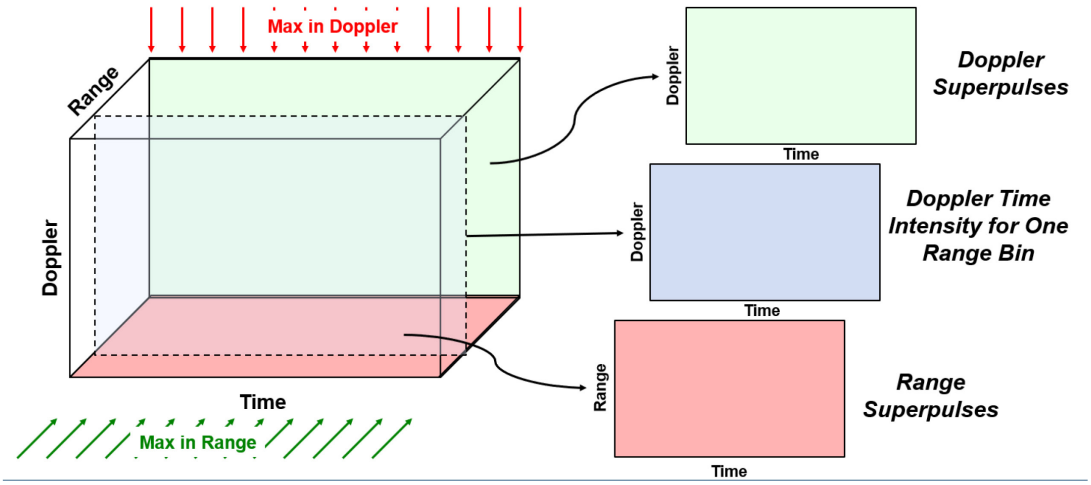

Figure 2: Looking through the range-doppler tensor.

Finally, looking through the top Range-Doppler face shows the maximum in each range-Doppler bin at any time during the dataset. This view shows the span of each targets' range and Doppler span during the processing window. We will refer to it as the Range-Doppler overview.

3.2 Multi-target Detection & Tracking

Figure 3 shows an example of Range-Doppler Tensor processing with WSRT data for the Nilesat (Object 36830) cluster in December 2022. Moving clockwise from the top-left, the figures are: a) a single range-Doppler map formed with four seconds of data; b) The Range Doppler Tensor with range on the x-axis, range-rate on the y-axis, and time on the z-axis; c) the range and Doppler overview of the targets throughout the collect; d) the Doppler superpulses; and e.) the Range superpulses. Figure 3 illustrates that from WSRT's perspective, the two of the three targets were initially close in range. During the collect, the targets moved to their range-crossover point, where the bistatic range between MHR, the targets, and WSRT was equal. However, the spread Figure 3e (the Range-Doppler overview) relative to Figure 3a (a single Range-Doppler map) shows that while all targets range and Doppler varied throughout the collect, their range and Doppler metrics never overlapped. Viewing the Doppler-Time face of the Range-Doppler tensor also shows that the targets are easily separated by their range-rates, which varied smoothly throughout the collection window. Any maneuver that changes a bistatic range-rate would quickly show up as a change to the slope of the Doppler Superpulses. Finally, the simple straight traces in Figure 3d show that all targets were stable throughout the collect.

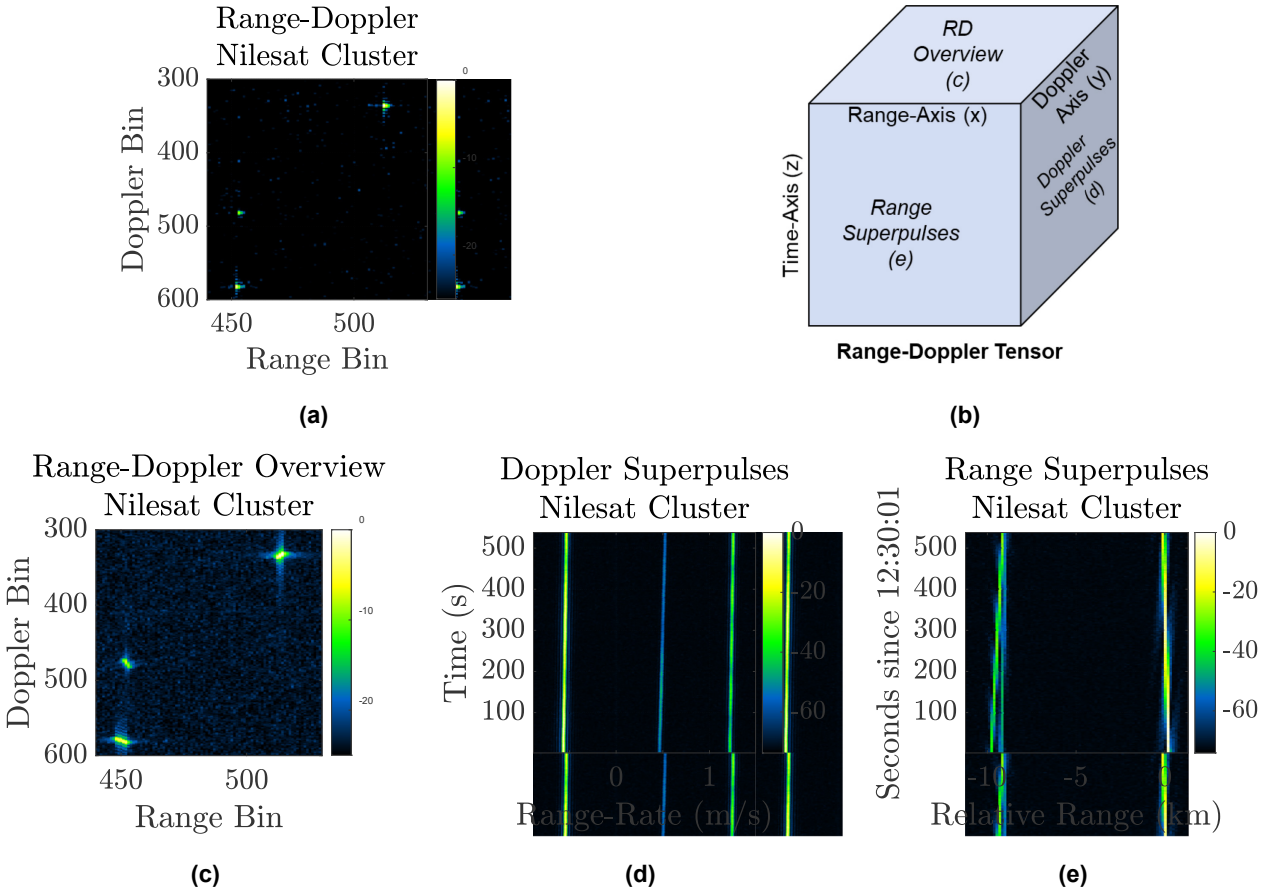

Figure 3: December 2022 Nilesat (object 36830) cluster viewed from WSRT. a) a single range-Doppler map formed with four seconds of pulses; b) The Range Doppler Tensor with range on the x-axis, range-rate on the y-axis, and time on the z-axis; c) the range and Doppler spans of the targets over the collect – the top face of the RD Tensor; d) the Doppler superpulses – the side face of the RD Tensor; and e.) the Range superpulses – the front face of the RD Tensor.

3.3 MHS Processing for Long Coherent Integration

Another processing option is to apply Multiple Hypothesis Search (MHS) for the longest possible interval. Finding the longest interval with ideal coherent gain will determine the minimum detectable RCS for a stable target. Long coherent integration also informs how well synchronized the transmitter and receiver clocks are. Figure 4 shows that MHR-WSRT maintained 3dB of gain per octave of CPI throughout the 540s collection for the two brighter targets. This indicates that the target's range walks can be well fit by a quadratic range-walk assumption. Coherence over the interval also shows that any drift between the transmitter and receiver clocks can be corrected by quadratic range-walk hypothesis. Nine minutes of ideal integration coherent integration adds about 43dB to the nominal SNR in Table 1. Further experiments are needed to evaluated the minimum detectable target level.

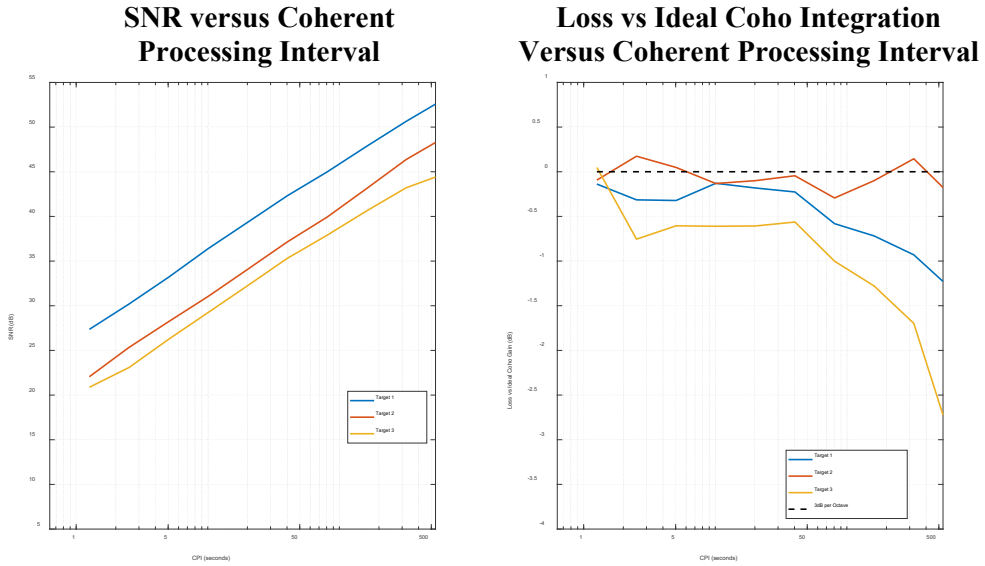

Figure 4: Target signal to noise ratio (left) and comparison to ideal versus coherent processing interval for the Nilesat cluster viewed from WSRT.

While the longest possible CPI determines the minimum detectable target, Measurement and Signal Intelligence (MASINT) and operational Space Surveillance Network systems often require multiple metric observations of GEO targets from shorter CPIs. Metric observations include target state and signature. With typical radar collections, signature includes RCS in the principal polarization (PP), the orthogonal polarization (OP), and the amplitude/phase ratio between PP and OP. Naturally, these coherent bistatic datasets can be divided into short CPIs and input into MHS. MHS estimates relative range, range-rate, and range-acceleration for each short CPI. Each CPI also yields an estimate of the PP and OP SNR and relative phase. These observations can be input to a multi-target tracker (MTT). An MTT will associate observations into tracks, then predict and update each track's state with each new observation from MHS.

Figure 5 shows the output from the multi-target tracker for the MHR-WSRT observation of the Nilesat cluster. Clockwise from the top left, the figures are relative range vs time; relative range-rate vs time; phase between the Principal Polarization (PP) and the Orthogonal Polarization (OP), OP SNR, and PP SNR. As expected from the range Doppler Tensor, the targets are easily separated in range and range-rate. In addition, the targets have unique SNR ratios between the PP and OP returns. Finally, the phase between the PP and OP returns vary slowly over time for these stable GEO targets. The bistatic data thus provides a rich dataset for satellite identification, change detection, and tracking that will improve space domain awareness at geo-synchronous orbits.

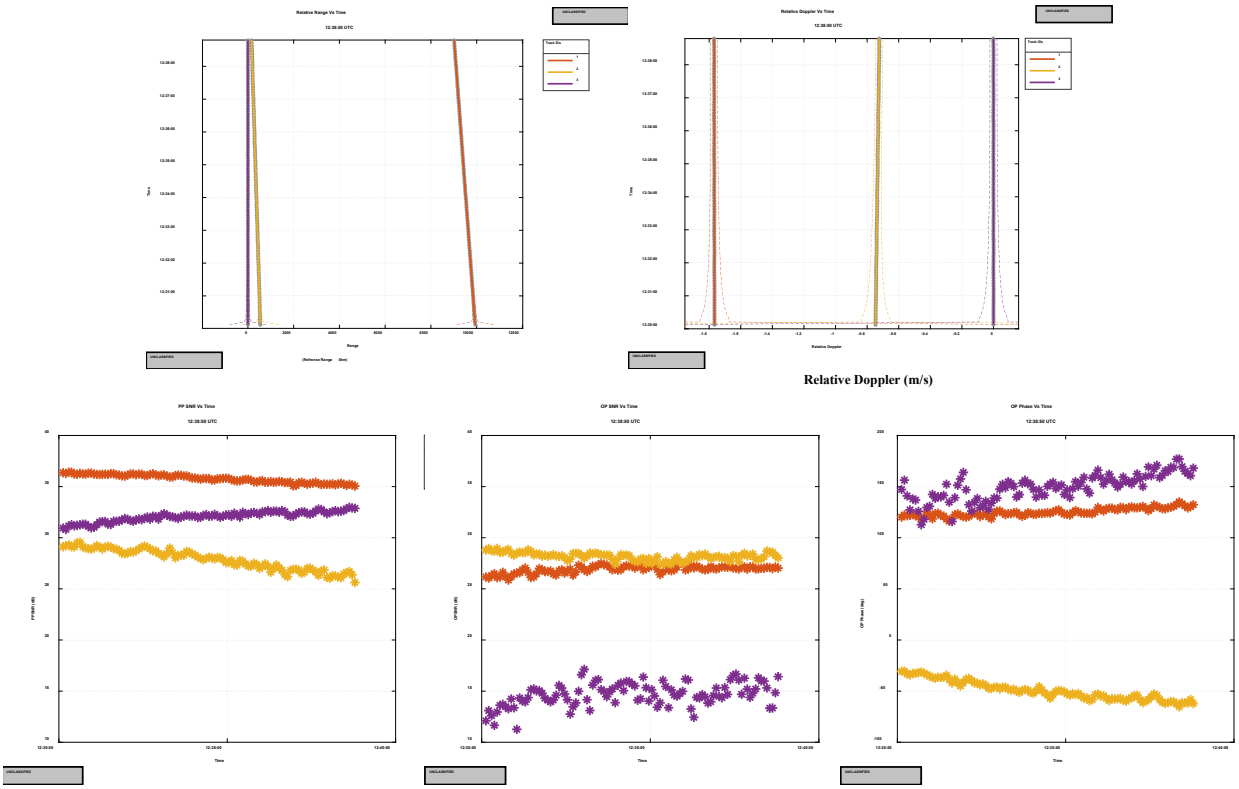

Figure 5: Multi-target tracking for the Nilesat cluster viewed from WSRT. Clockwise from the top left, the plots show relative range; relative range-rate; relative phase between the OP and PP returns for each target; OP SNR vs time; and PP SNR vs Time.

3.4 Tumbling Target Doppler Processing and Characterization

The Range-Doppler tensor is also the starting point for Doppler characterization. The December 2022 collect also looked at a tumbling Delta 4 Rocket Body, Space Catalog Number 40535. Details of the second stage of a Delta 4 Rocket Body are shown in Figure 6.

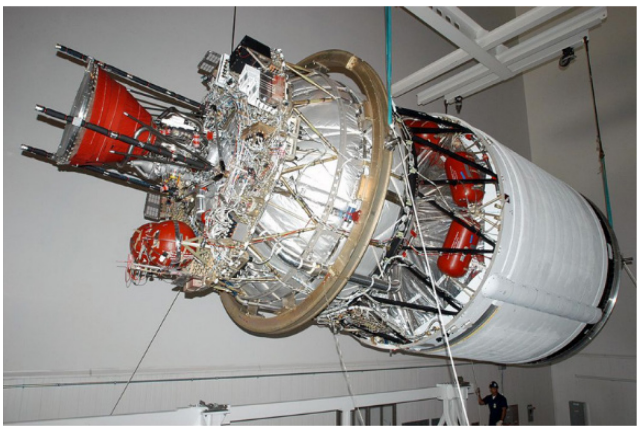

Height	12.2 m
Diameter	4 m
Empty Mass	2,850 kg

Figure 6: Delta 4 rocket body ground truth.

The rocket body was illuminated by MHR, while WSRT and the Cambridge, Darnhall, Defford, and Knockin receivers of the Jodrell Bank Observatory (JBO) recorded. The Delta 4 is not a GEO target and hence significant range and range rate migration need to be accounted for in order to stabilize the target. This

was done by a manual optimization of the range rate parameters (and a completely independent data processing chain) yielding a residual Doppler spectrogram shown in Figure 7. The flashes from specular reflections and the sinusoidal variations clearly indicate a tumbling target with a period of approximately 160 seconds. This spectrogram is also known as the micro-Doppler signature of the Delta 4 Rocket body.

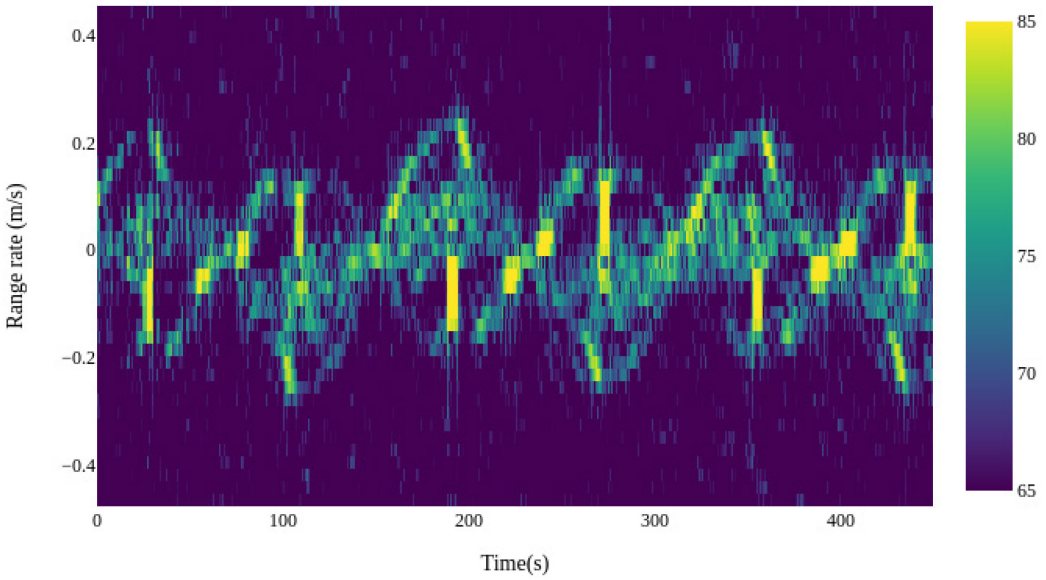

Figure 7: Detailed Micro-doppler signature of the Delta4 rocket body as seen from the Darnhall receiver. All partners carried out independent processing of the receiver data.

Superpulse processing was applied to all the participating e-MERLIN receivers (Cambridge, Defford, Knockin, Darnhall) and the resulting spectrograms are shown in Fig 3.7 with improved SNR. The similarity of the results across different receive antennas and processing chains demonstrates the robustness of the method, but small differences between well-separated receivers may also be exploited.

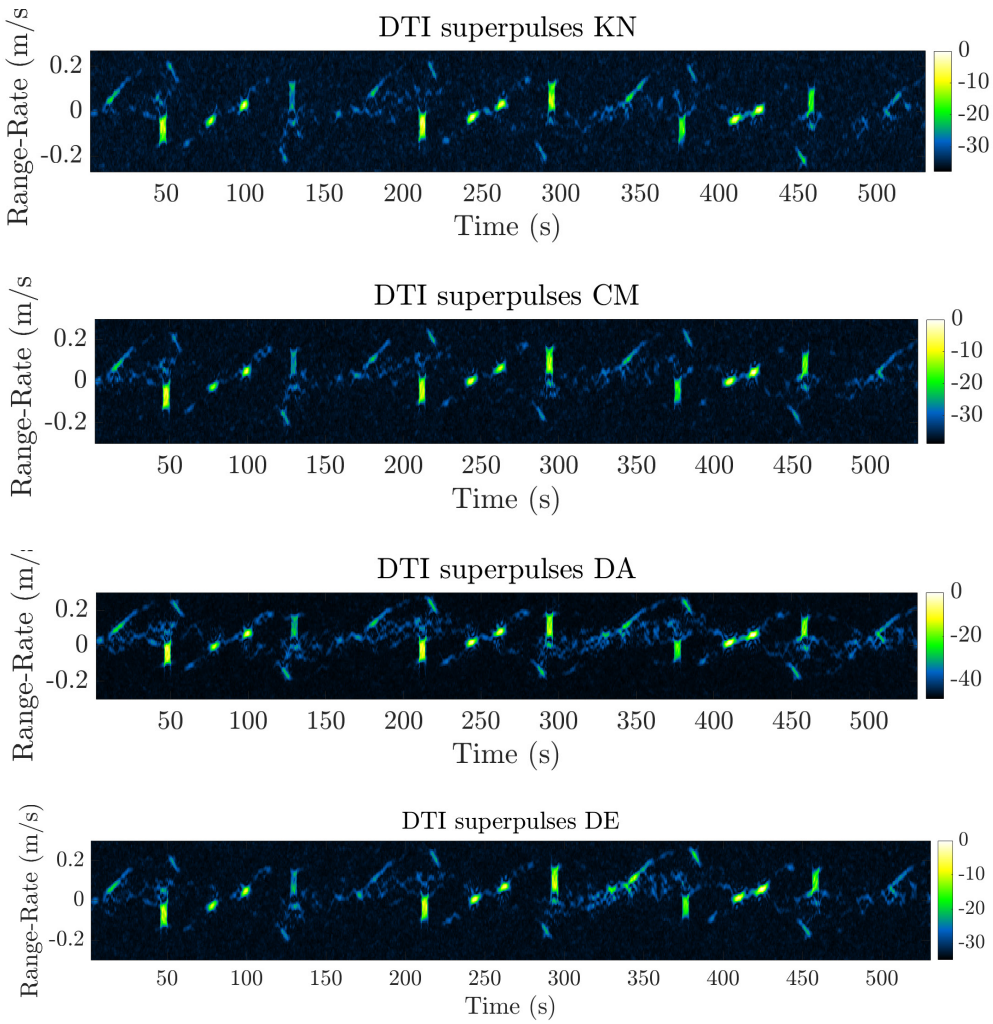

Figure 8: Principal polarization Doppler superpulses for the December 2022 collect on a tumbling Delta 4 rocket body. The Knockin, Cambridge, Darnhall, and Defford receivers of JBO are shown.

The stabilized Doppler superpulses are the starting point for Tomographic characterization of the Delta 4. Tomography is made possible by to the principle that point scatterers on a line of constant cross-range will reflect back echoes that share the same Doppler-shifted frequency [17]. Consequently, Doppler profiles can be parametrized in terms of cross-range position and aspect angle view of the object. Tomographic image reconstruction techniques can utilize for Doppler tomography such as Filtered Back Projection (FBP) [18]. FBP reconstructions formed using the logarithmic power of the Doppler profiles are shown in Figure 9. The FBP reconstructions show that the range extent of the illuminated target agrees with the expected 12.2m length of the Delta 4 second stage. The image planes from the various aspect angles of the JBO – as well as from MHR – may be useful in 3D model reconstruction of the illuminated target.

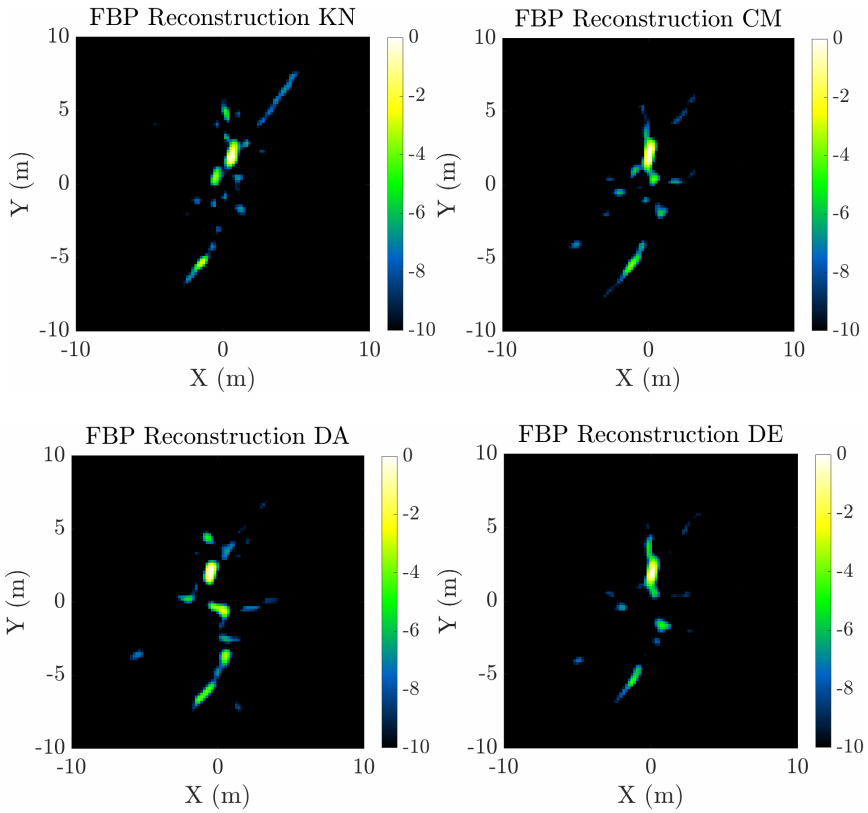

Figure 9: Tomographic image reconstructions of the Delta 4 rocket body from the Jodrell Bank Observatory. Clockwise from the top-left, reconstructions are shown for Knockin, Cambridge, Darnhall, and Defford receivers.

Similar to FBP, the use of Inverse Radon Transform (IRT) was also investigated for obtaining Tomographic Image Reconstructions [19]-[20]. Specifically, reconstructions based on the Spectrogram Inverse Radon based Transform Algorithm (SIRTA) are presented in Figure 10. The SIRTA method relies on a Concentration Measure [21] to select the period from a vector of candidate periods. In order to reduce the set of candidates an initial guess is made by exploiting the autocorrelation function of the signal [22]. The reconstructions obtained through SIRTA exhibit a high level of agreement with those obtained through FBP, providing additional confidence in the accuracy of the results. It is worth noting that the results in Figure 10 were obtained using the rotation period estimated by the SIRTA estimation loop, with values of 165.5766s, 165.2404s, 163.7705s, and 165.1222s obtained for the Knockin, Cambridge, Darnhall, and Defford receiver data, respectively. Therefore, in addition to observing agreement in the estimated sizes, consistency in the estimation of the rotation period is also found. It is worth noting that for the reconstructions depicted in Figure 10, the compensation of the target phase of the received signal was achieved by using Image Contrast-Based Autofocus (ICBA) [23], a widely used autofocus technique for ISAR image formation.

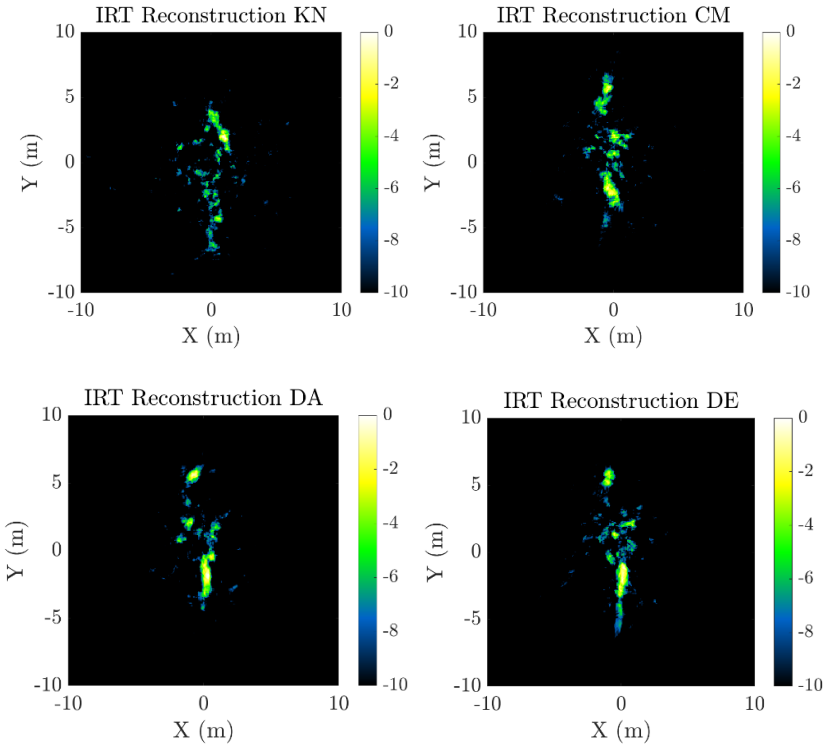

Figure 10: SIRTA reconstructions of the Delta 4 rocket body. Clockwise from the top-left, reconstructions are shown for Knockin, Cambridge, Darnhall, and Defford receivers of JBO.

Furthermore, The University of Manchester's Jodrell Bank Observatory carried out their own independent processing of the receiver data, using completely separate software and reproduced similar FBP/IRT images, which are not shown for brevity. Assessments of object size and tumble rate were the same among all partners. Consistent agreement between independent processing pipelines shows that engaging NATO partners will improve our dynamic understanding of space activities in or near Geosynchronous orbits (GEO).

4.0 CONCLUSIONS

Successful continental-baseline bistatic radar collections on GEO targets have demonstrated long coherent integration times, multi-target detection and tracking and characterization of a tumbling object.

Achieving long, coherent, integration intervals, exceeding 540 seconds and 27K pulses, was enabled by accurate orbit determination using the Multi-Hypothesis Search (MHS) technique. Using MHS to determine detailed orbital motions of multiple objects in the bistatic beams enabled multi-target tracking of the various objects which matched to their orbital element sets. This capability is of particular interest to military SDA as it can be used to understand satellite behavior in closely spaced, or satellite cluster environments. This capability was achieved in all of the year-2022 experiments which included observations of multiple GEO clusters, such as the Intelsat 37E cluster, in which all objects seen in the monostatic data are detected on multiple telescopes in the bistatic data.

Another application of Range-Doppler processing (beyond MHS) is for object characterization. Using modest integration intervals and examining the target motion over time, it was shown that characteristics of a tumbling rocket body could be obtained, including the object's size, shape, and rate of tumble employing multiple, independent tomographic algorithms. Further analysis can yield 3-D object imaging and multi-

lateral position estimation. The example shown in this paper is on a tumbling object, but these techniques could be extended to evaluate maneuvering objects or ones in performing rendezvous and proximity operations which is of significant SDA value.

Future plans for SET-293 activities include collections with calibration targets, such as the ETALON spheres, in order to determine sensor biases and propagation delays, and to determine the measured bistatic signal-to noise gain of each sensor to accurately determine bistatic RCS. Additional data collections have already been conducted in 2023 under the NATO SET-293 effort and more are planned. There has been a desire from the outset of the RTG to investigate bistatic capability at higher frequencies than L-band. The existing large dish receiver at Goonhilly, UK is currently incorporating a new X-band receiver which will enable bistatic collections with the high power HUSIR X-band radar operated by MIT Lincoln Laboratory (USA). Initial collections occurred in February of 2023.

Bistatic radar, especially with large, highly sensitive radio telescopes remains a promising and low-cost way to achieve increased sensitivity, multi-target tracking and satellite characterization in the GEO regime.

5.0 ACKNOWLEDGMENTS

The authors wish to acknowledge the NATO Sensors, Electronics and Technology (SET) Research Panel, and the United States Space Command J2 Chief Technology Officer for sponsoring this research. The Jodrell Bank Observatory and e-MERLIN are operated by the University of Manchester on behalf of UK Research and Innovation and has received funding from the European Union's Horizon 2020 research and innovation programme under grant agreement No 101004719 . This work makes use of data from the Westerbork Synthesis Radio Telescope owned by ASTRON, the Netherlands Institute for Radio Astronomy. The authors would like to also thank Netherlands Organization for Applied Scientific Research (TNO) for technical discussions.

The authors also wish to thank the sensor operations teams: Jeffrey Kemp, Linda Beebe, Madison Lagos and Christine Melcher from MHR; and Richard Blaauw from WSRT.

6.0 REFERENCES

[1] United States Defense Intelligence Agency, "2022 Challenges to Security in Space," 2022, III. https://www.dia.mil/Portals/110/Documents/News/Military_Power_Publications/Challenges_Security_Space_2022.pdf.

[2] NATO's overarching Space Policy, https://www.nato.int/cps/en/natohq/official_texts_190862.htm.

[3] United States Space Command (USSPACECOM) Organizational Fact Sheet, https://www.spacecom.mil/Portals/32/USSPACECOM%20Fact%20Sheet%2018Jun20.pdf?ver=2020-06-18-155219-363.

[4] D. DeBoer and D. Bock, "The allen telescope array: splitting the aperture," IEEE Microwave Magazine, vol. 5, no. 2, pp. 46–53, 2004.

[5] Duev, D, Molera-Calves, G, Pogrobenko, S et al (2012) Astronomy & Astrophysics, Volume 541, 43.

[6] N. Willis, Bistatic Radar. Boston, London: Artech House, 1991.

[7] Welch, S, Hogan G, et al, "Long Baseline Bistatic Measurements of Geostationary Satellites", European MicroWave Week, September 2022.

[8] Welch, S, Hogan G, et al, "Long Baseline Bistatic Measurements for Space Situational Awareness", NATO SCI-SET-297 Specialists' Meeting on Space Situational Awareness, October 2022.

[9] Lincoln Laboratory, Massachusetts Institute of Technology. (2022) Lincoln Space Surveillance Complex. [Online]. Available: https://www.ll.mit.edu/about/facilities/lincoln-space-surveillance-complex.

[10] M. Richards, Fundamentals of Radar Signal Processing. New York, NY: McGraw-Hill, 2005, Ch. 4.

[11] C. V. Jakowatz, D. E. Wahl, P. H. Eichel, D. C. Ghiglia, and P. A. Thompson, Spotlight-Mode Synthetic Aperture Radar: A Signal Processing Approach. Boston, MA: Springer US, 1996, pp. 1–31.

[12] K. Letsch, L. Leushacke1, J. Rosebrock1, R. Jehn, H. Krag, and R. Keller, First Results from the Multibeam Bistatic Beampark Experiment at FGAN, 5th European Conference on Space Debris, 2009.

[13] D. Mehrholz, Radar Observations of Geosynchronous Orbits, 2nd European Conference on Space Debris, 1997.

[14] D. Cerutti-Maori, J. Rosebrock, C. Carloni, M. Budoni, I. Maouloud, and J. Klare, "A Novel High-Precision Observation Mode for the Tracking and Imaging Radar TIRA – Principle and Performance Evaluation – ", 8nd European Co1nference on Space Debris, 2021.

[15] R. E. Blahut, "Theory of Remote Image Formation," Cambridge University Press (2004).

[16] A. Serrano and R. L. Morrison, "Doppler Superpulse Processing for Improved Tomographic Characterization of Space Objects", 2023 International Applied Computational Electromagnetics Society Symposium (ACES), Monterey, CA, USA, 2023, (forthcoming).

[17] D. L. Mensa, S. Halevy, and G. Wade, "Coherent Doppler tomography for microwave imaging," Proc. IEEE, vol. 71, no. 2, p. 254, Feb. 1983.

[18] A. Kak and M. Slaney, *Principles of Computerized Tomographic Imaging*. IEEE Press, 1988.

[19] S.Ghio, M.Martorella: "Estimation of Rotating RSO Parameters using Radar Data and Joint Time-Frequency Transforms", 7th European Conference on Space Debris ESA/ESOC, April 2017.

[20] S.Ghio, M.Martorella, D.Staglianò, D.Petri, S.Lischi, R. Massini: " Practical implementation of the Spectrogram-Inverse Radon Transform based Algorithm for RSO parameter estimation", IET Science, Measurement & Technology, August 2019.

[21] Stankovic L., (2003). Measuring Time-Frequency distributions concentration, in Time-Frequency Signal Analysis and Processing, Elsevier, 1820-1825.

[22] Ghio, S.; Martorella, M.; Staglianò, D.; Petri, D.; Lischi, S.; Massini, R. Experimental Comparison of Radon Domain Approaches for Resident Space Object's Parameter Estimation. Sensors 2021, 21, 1298. https://doi.org/10.3390/s21041298.

[23] Martorella, M.; Berizzi, F.; Haywood, B.:'Contrast maximisation based technique for 2-D ISAR autofocusing', IEE Proceedings - Radar, Sonar and Navigation, 2005, 152, (4), p. 253-262, DOI: 10.1049/ip-rsn:20045123.